REVIEW ARTICLE

Photoexcited electron and hole dynamics in semiconductor quantum dots: phonon-induced relaxation, dephasing, multiple exciton generation and recombination

Kim Hyeon-Deuk[1] **and Oleg V. Prezhdo**[2]

[1]Department of Chemistry, Kyoto University, Kyoto, 606-8502, Japan
[2]Department of Chemistry, University of Rochester, Rochester, NY 14642, USA

E-mail: kim@kuchem.kyoto-u.ac.jp, oleg.prezhdo@rochester.edu

Abstract. Photoexcited dynamics of electrons and holes in semiconductor quantum dots (QD), including phonon-induced relaxation, multiple exciton generation, fission and recombination (MEG, MEF, and MER), were simulated by combining *ab initio* time-dependent density functional theory and non-adiabatic molecular dynamics. These nonequilibrium phenomena govern optical properties and photoexcited dynamics of QDs, determining the branching between electronic processes and thermal energy losses. Our approach accounts for QD size and shape as well as defects, core-shell distribution, surface ligands, and charge trapping, which significantly influence the properties of photoexcited QDs. The method creates an explicit time-domain representation of photoinduced processes and describes various kinetic regimes owing to the non-perturbative treatment of quantum dynamics. QDs of different size and material, with and without ligands are considered. The simulations provide direct evidence that the high-frequency ligand modes on the QD surface play a pivotal role in the electron-phonon relaxation, MEG, MEF, and MER. The insights reported here suggest novel routes for controlling the photoinduced processes in semiconductor QDs and lead to new design principles for increasing efficiencies of photovoltaic devices.

1. Introduction

Confinement of charge carriers in quantum dots (QDs) of sizes smaller than the Bohr exciton radius of the corresponding bulk material gives the ability to control the electronic properties by variation of QD size and shape, and leads to a variety of applications.[1,2] QDs are in sharp contrast with molecular systems, whose properties vary discontinuously and require modifications in composition and structure. Large absorption cross sections, decreased electron-phonon relaxation rates,[3,4] and generation of multiple electron-hole pairs[5–9] make QDs excellent photovoltaic materials by providing new mechanisms for utilization of the photon energy in excess of the band gap and avoiding energy losses.[3,10]

Typically, significant amounts of solar power are lost to heat, limiting the maximum thermodynamic efficiency of a standard photovoltaic device to 32%.[11] Recent time-resolved experiments showed ultrafast electron-phonon relaxation even in nanoscale QDs, similar to that observed in bulk.[12–17] The general expectation that quantum confinement would limit energy losses due to an increased mismatch between the electronic energy gaps and phonon frequencies held only at low energies and in perfectly designed QDs.[4] Photovoltaic and lasing efficiencies of QD materials depend critically on the rates of electron-hole energy exchange and charge-phonon relaxation. Therefore, studying electron-hole and charge-phonon interactions carry both fundamental and practical importance.[18]

Electron-phonon interactions are responsible for two related but qualitatively different phenomena, *i.e.*, relaxation and dephasing. The former is an inelastic process, leading to energy losses. Such energy losses decrease solar cell voltage. At the same time, fast relaxation of higher energy excited states to band gap edge favors lasing and electro-optic switching. Electron-phonon dephasing is an elastic process and conserves the electronic energy. It destroys coherences between electronic states, converting them into uncorrelated ensembles. Quantum information processing requires long-lived coherences and slow phonon-induced dephasing of spin and electron states. Dephasing determines homogeneous linewidths in optical spectra. The loss of correlation in coherent superpositions of multiple excitons (MEs) contributes to ME fission (MEF) that is closely related to the singlet fission process in polyacene crystals.[19,20] Phonon-induced dephasing of coherent superpositions of single and ME states is an essential component of the mechanism for ME generation (MEG).[8,19,21,22]

MEG creates multiple charge carriers by a single photon absorption, and provides potential for increasing photovoltaic device efficiencies.[9,23,24] MEG has been observed in semiconductor QDs[5–8,21,25–40] and other nanoscale materials.[41–45] MEG yields are generally higher in QDs than in bulk,[9,24,46] because strict conservation of translational momentum is not required in QDs, and the Coulomb interaction between electrons and holes is enhanced due to closer proximity of charge carriers. On the contrary, multiple exciton recombination (MER), in combination with electron-phonon relaxation, reduces photovoltaic efficiencies by accelerating energy losses to heat. MEs convert to single

excitons (SEs) of higher energy that is ultimately dissipated by phonons.[6,18,37,47–52] In combination with electron-phonon relaxation, the MEG and MER govern photoexcited-state dynamics in semiconductor QDs at high energies.[5,6]

Recent experiments reported enhanced photon-to-charge conversion due to MEG in PbSe QD-based solar cells, as manifested by increased photocurrent.[40,53] This result indicates that understanding the MEG and MER phenomena appearing in QDs can help in developing efficient solar technology. At the same time, the diverse and conflicting reports on MEG efficiencies show that the dynamics and mechanisms of MEG and MER are still poorly understood and remain controversial.[46,54–60] In particular, surface-induced charge trapping and related processes are believed to be the source of the discrepancies in the MER and MEG signals and their interpretation.

This paper reviews recent state-of-the-art time-domain *ab initio* simulations of the properties and dynamics of photoexcited states in semiconductor QDs including charge-phonon relaxation, MEG, MEF, and MER, as shown in figure 1.[5,6,18,19] The atomistic and time-domain description created by our method provides a powerful tool for studying the role of surface ligands, dopants, defects, unsaturated chemical bonds, size, shape, and other realistic aspects of QDs. The described simulations give a novel and comprehensive perspective on the elastic and inelastic scattering dynamics of photoexcited charge carriers in nanoscale materials and provide important insights into the mechanisms and efficiency of solar energy harvesting.

2. Theoretical framework

We first summarize our theoretical methods which enable the current time-domain *ab initio* simulation to study the photoexcited dynamics in semiconductor QDs.

2.1. Time-domain density functional theory

Our state-of-the-art simulations combine time-domain density functional theory (TDDFT) with non-adiabatic molecular dynamics (NAMD).[6,14,18,61,62] The electronic structure and adiabatic MD were computed with VASP[63] using a converged plane-wave basis in a cubic simulation cell periodically replicated in three dimensions. Spurious interactions of periodic images were prevented by including at least 8 Å of vacuum between QD replicas. The PW91 density functional and projector-augmented-wave pseudopotentials were used. Note that hybrid DFT functionals, as well as the GW and Bethe-Salpeter theories, tend to produce larger band-gaps. We use the PW91 functional in order to take full computational advantage of the plane-wave representation. Preserving computational efficiency is particularly important for our real-time TDDFT simulations that include explicit couplings to phonon modes. The initial QD geometry was generated from bulk, passivated by hydrogen atoms as needed, fully optimized at zero temperature, and heated up to ambient temperatures by MD with repeated nuclear kinetic energy rescaling. Microcanonical trajectories of 5 ps to

30 ps were produced using the Verlet algorithm with a 1 fs time-step and the Hellman-Feynman force in the ground electronic state.

The evolution of the single-electron Kohn-Sham (KS) orbitals $\phi_{\rm p}(\boldsymbol{r},t)$ was determined using the standard TDKS equations

$$i\hbar\frac{\partial\phi_{\rm p}(\boldsymbol{r},t)}{\partial t} = H(\phi(\boldsymbol{r},t))\phi_{\rm p}(\boldsymbol{r},t), \quad p=1,\ldots,N_{\rm e}, \tag{1}$$

where $N_{\rm e}$ is the number of electrons. The equations are coupled, since the Hamiltonian H depends on the density obtained by summing over all the KS orbitals occupied by the $N_{\rm e}$ electrons. Expanding the time-dependent KS orbitals $\phi_{\rm p}(\boldsymbol{r},t)$ in the adiabatic KS orbital basis $\tilde{\phi}_{\rm k}(\boldsymbol{r};\boldsymbol{R})$,

$$\phi_{\rm p}(\boldsymbol{r},t) = \sum_{\rm k=1}^{N_{\rm e}} c_{\rm pk}(t)|\tilde{\phi}_{\rm k}(\boldsymbol{r};\boldsymbol{R})\rangle, \tag{2}$$

transforms the TDKS equations (1) into the equations for the expansion coefficients

$$i\hbar\frac{\partial c_{\rm pk}(t)}{\partial t} = \sum_{\rm m=1}^{N_{\rm e}} c_{\rm pm}(t)(\epsilon_{\rm m}\delta_{\rm km} - i\hbar\boldsymbol{d}_{\rm km}\cdot\dot{\boldsymbol{R}}). \tag{3}$$

The adiabatic KS orbitals, $\tilde{\phi}_{\rm k}(\boldsymbol{r};\boldsymbol{R})$, were obtained with DFT for atomic positions at each time step along the MD trajectory. The NA coupling describes the electron-phonon interaction

$$\boldsymbol{d}_{\rm km}\cdot\dot{\boldsymbol{R}} = \langle\tilde{\phi}_{\rm k}(\boldsymbol{r};\boldsymbol{R})|\nabla_{\boldsymbol{R}}|\tilde{\phi}_{\rm m}(\boldsymbol{r};\boldsymbol{R})\rangle\cdot\dot{\boldsymbol{R}} \tag{4}$$

$$= \langle\tilde{\phi}_{\rm k}(\boldsymbol{r};\boldsymbol{R})|\frac{\partial}{\partial t}|\tilde{\phi}_{\rm m}(\boldsymbol{r};\boldsymbol{R})\rangle. \tag{5}$$

The NA electron-phonon coupling arises due to the dependence of the adiabatic KS orbitals on the phonon dynamics $\boldsymbol{R}(t)$. Nuclear trajectories from the ground state MD were used to sample initial conditions to create ensemble averages for the NA dynamics.

2.2. NAMD simulation: fewest switching surface hopping

Fewest switching surface hopping (FSSH)[10,14,18,62,64,65] prescribes a probability for hopping between quantum states. Specifically, the probability of a hop from a given state k to another state m within the time interval $\mathrm{d}t$ is given by

$$\mathrm{d}P_{\rm km} = \frac{b_{\rm km}}{a_{\rm kk}}\mathrm{d}t, \tag{6}$$

where

$$b_{\rm km} = -2\mathrm{Re}(a_{\rm mk}\boldsymbol{d}_{\rm mk}\cdot\dot{\boldsymbol{R}}) \tag{7}$$

$$a_{\rm mk} = c_{\rm m}^{*}c_{\rm k}. \tag{8}$$

Here, $c_{\rm k}$ and $c_{\rm m}$ are coefficients evolved by (3). The velocity rescaling and hop rejection rules in FSSH give detailed balance between the upward and downward transitions.[66] A simplified version of these rules assumes that energy exchanged between the electronic and nuclear degrees of freedom during a hop is rapidly redistributed over all nuclear modes. With this assumption, energy of the nuclear modes follows a Boltzmann

distribution at all times, and the velocity rescaling/hop rejection step can be replaced by multiplying the probability, (6), for transitions upward in energy by the Boltzmann factor. This simplification of the original FSSH technique provides great computational savings.[67]

2.3. Theory for calculating dephasing times

The vibrationally-induced dephasing times are computed using the optical response function formalism.[68] The dephasing time is associated with fluctuations of the energy levels due to coupling of electrons and holes to phonons of the semiconductor, vibrations of the ligands, motion of the solvent, etc. The fluctuations in the energy levels are best characterized in terms of correlation functions. The normalized autocorrelation function (ACF) for time-dependent energy $E(t)$ is defined as

$$C(t) = \frac{\langle \Delta E(t) \Delta E(0) \rangle}{\langle (\Delta E(0))^2 \rangle}. \tag{9}$$

where $\Delta E(t) \equiv E(t) - \langle E(t) \rangle$, and the angular brackets denote averaging over a statistical ensemble. ACFs characterize periodicity and memory of the energy fluctuations. Rapid decay of an ACF indicates short memory and occurs if multiple and anharmonic phonon modes couple to the electronic transition. The optical response functions characterizing the dephasing processes for a pair of states that are entangled in a coherent superposition can be obtained directly or via the second order cumulant expansion.[68] The cumulant dephasing function is obtained by double integration and exponentiation of the unnormalized ACF,

$$D(t) = \exp\left[-\frac{1}{\hbar^2} \int_0^t d\tau_1 \int_0^{\tau_1} d\tau_2 \langle (\Delta E(0))^2 \rangle C(\tau_2) \right]. \tag{10}$$

The above expression indicates that rapid dephasing is facilitated by a large fluctuation of the transition energy, $\langle (\Delta E(0))^2 \rangle$, as well as by a short memory of the fluctuation, *i.e.* rapidly decaying ACF. The dephasing times were calculated by fitting the dephasing function by a Gaussian function.

2.4. Time-dependent density functional theory for MEG and MER

The Auger dynamics involving SE and double exciton (DE) states coupled to nuclear motions were simulated using TDDFT formulated in the adiabatic KS basis.[6,14,18,61] In the adiabatic representation, all Coulomb interactions appearing in the electronic Hamiltonian are "diagonalized out" during the calculation of the adiabatic states, and transitions between different SE and DE states occur due to the NA coupling, as described below.

Our simulation method including the ground, SE, and DE states, $|\Phi_{\rm g}(\boldsymbol{r};\boldsymbol{R})\rangle$, $|\Phi_{\rm SE}^{\rm i,j}(\boldsymbol{r};\boldsymbol{R})\rangle$, and $|\Phi_{\rm DE}^{\rm i,j,k,l}(\boldsymbol{r};\boldsymbol{R})\rangle$, respectively, was formulated using second quantization with the ground state as a reference.[6] SEs and DEs are obtained as

$$|\Phi_{\rm SE}^{\rm i,j}\rangle = \hat{a}_{\rm i}^{\dagger}\hat{a}_{\rm j}|\Phi_{\rm g}\rangle \tag{11}$$

$$|\Phi_{\rm DE}^{\rm i,j,k,l}\rangle = \hat{a}_{\rm i}^{\dagger}\hat{a}_{\rm j}\hat{a}_{\rm k}^{\dagger}\hat{a}_{\rm l}|\Phi_{\rm g}\rangle, \tag{12}$$

where the electron creation and annihilation operators, $\hat{a}_{\rm i}^{\dagger}$ and $\hat{a}_{\rm j}$, generate and destroy an electron in the ith and jth adiabatic KS orbitals, respectively. The time-evolving wave function is then expressed by

$$|\Psi(t)\rangle = C_{\rm g}(t)|\Phi_{\rm g}\rangle + \sum_{\rm i,j} C_{\rm SE}^{\rm i,j}(t)|\Phi_{\rm SE}^{\rm i,j}\rangle + \sum_{\rm i,j,k,l} C_{\rm DE}^{\rm i,j,k,l}(t)|\Phi_{\rm DE}^{\rm i,j,k,l}\rangle. \tag{13}$$

Similarly to (3), the expansion coefficients appearing in (13) evolve by the first-order differential equations

$$\begin{aligned} i\hbar\frac{\partial C_{\rm X}(t)}{\partial t} &= C_{\rm X}(t)E_{\rm X} - i\hbar C_{\rm g}(t)\boldsymbol{d}_{\rm X;g}\cdot\dot{\boldsymbol{R}} - i\hbar\sum_{\rm i',j'} C_{\rm SE}^{\rm i',j'}(t)\boldsymbol{d}_{\rm X;SE,i',j'}\cdot\dot{\boldsymbol{R}} \\ &\quad - i\hbar\sum_{\rm i',j',k',l'} C_{\rm DE}^{\rm i',j',k',l'}(t)\boldsymbol{d}_{\rm X;DE,i',j',k',l'}\cdot\dot{\boldsymbol{R}}, \end{aligned} \tag{14}$$

where X and Y now correspond to either ground, SE, or DE state, $E_{\rm X}$ is the state energy, and the NA couplings are defined by

$$\boldsymbol{d}_{\rm X;Y}\cdot\dot{\boldsymbol{R}} \equiv \langle\Phi_{\rm X}|\nabla_{\boldsymbol{R}}|\Phi_{\rm Y}\rangle\cdot\dot{\boldsymbol{R}} \tag{15}$$

$$= \langle\Phi_{\rm X}|\frac{\partial}{\partial t}|\Phi_{\rm Y}\rangle. \tag{16}$$

The atomistic simulation of the SE/DE generation and recombination dynamics was performed by directly solving (14) with time-dependent NA couplings and energies calculated by VASP.[5,6] We developed efficient simulation codes to solve (14) using only the extracted non-zero parts of the Hamiltonian.

Our method differs from other approaches such as the conventional Fermi's golden rule[31,33,34,44] by simultaneously taking into account MEG, MER, and phonon-assisted processes in a real-time atomistic simulation. The atomistic simulation allows us to study the roles of surface ligands, dopants, defects, unsaturated chemical bonds, size, shape, and other realistic properties of QDs in the MEG and MER dynamics. The NA coupling terms are calculated non-perturbatively in our simulation, leading to non-exponential MEG and MER dynamics. This bypasses the limitations of Fermi's golden rule that adopts perturbative treatment and implicitly assumes exponential decay. Additionally, the present explicit time-domain simulations account for phonon dynamics, including high-frequency surface ligand modes. Simulating dynamics with electron-phonon coupling creates fluctuations in the electronic energy levels responsible for dephasing of superpositions of SE and DE states, and allows for phonon-assisted MEG and MER. These phenonena are typically omitted in static rate theories.

3. Ultrafast charge cooling in semiconductor quantum dots by coupling to phonons

Quantum confinement in QDs induces larger electronic gaps and could cause mismatches between the energy gaps and phonon frequencies.[3] Phonon bottlenecks slow electron-phonon relaxation and were expected in QDs. However, only picosecond relaxations, similar to that observed in bulk, were observed in many time-resolved experiments,[16,17]

and a phonon bottleneck was detected only under special conditions in carefully designed CdSe QDs.[4,14]

Figure 2 presents the simulated NA dynamics of the electron and hole relaxation for the $Cd_{33}Se_{33}$ QD without surface passivation.[14] The three-dimensional figure shows the evolving state occupations, representing time-dependent distributions of electron and hole energies, as the particles relax to the corresponding band gap states. This reveals that the phonon bottleneck appears around the band edge of conduction band (CB), as the electron relaxation slows down at low energies. If the QD was passivated by ligands, the phonon bottleneck would be suppressed due to participation of the high-frequency phonon modes of the ligands and the resulting stronger NA couplings. In addition, the Auger exchange of energy between electrons and holes would be increased in the surface passivated QD.[69,70] In the following sections, the importance of the ligand contribution to the charge-phonon relaxation and Auger processes will be confirmed and discussed on the basis of our time-domain simulation studies.[10,14,18,65]

3.1. Density of electron and hole

The following discussion focuses on a small Si QD passivated by hydrogen atoms. Si is one of the most commonly used semiconductor materials, while hydrogen atoms represent the simplest realistic ligand. The upper panel of figure 3 shows the density of states (DOS) of $Si_{29}H_{24}$ at ambient temperature. The energy gap was calculated as 2.51 eV at 0 K. The underlying atomic structure, thermal fluctuations, as well as the Coulomb interactions break the electronic degeneracy, creating a complicated multilevel band structure and a distribution of energies for each state. To represent the inhomogeneous broadening, each energy level in the shown DOS was broadened by 0.1eV. Note that our time-domain simulation used band structure calculated for each instantaneous geometry along the trajectory and containing discrete energy levels. The quasi-continuous DOS suggests ultrafast relaxation of photoexcited electrons and holes, without a phonon bottleneck. The figure also demonstrates that the electron and hole DOS is symmetric due to the quantum confinement; the electron DOS is twice as dense as the hole DOS in bulk Si.[71] Such strong confinement effect on the DOS has not been observed in other semiconductor QDs such as PbSe and CdSe, in which the QD DOS is similar to the bulk DOS.[14,35,65]

3.2. Electron and hole relaxations

The lower panel of figure 3 shows relaxation rates of excited electrons and holes. In spite of the symmetric DOS of electrons and holes, the electrons decay much faster than the holes. The relaxation rates exhibit a nearly perfect linear relationship with the DOS, spanning the initially excited state to the band edge exciton. Not only are the absolute values of the relaxation rates larger for electrons than holes, but also the slope of the rate dependence on DOS is larger for electrons than holes.

3.3. Fermi's golden rule for electron-phonon relaxation

The above linear relationships are related to Fermi's golden rule:

$$k_{\mathrm{F}} = \frac{2\pi}{\hbar}|V|^2\rho(E_{\mathrm{band}}), \tag{17}$$

where k_{F} is the relaxation rate of the charge carriers, V is the electron/hole phonon coupling, and ρ is the density of electron and hole states. Using the NA coupling calculated from our simulation, Fermi's golden rule reproduces the electron relaxation data of figure 3. For hole relaxation, Fermi's golden rule holds when applying a constant prefactor of 0.53–the prefactor is rationalized by coupling fluctuations. NA coupling was for the first time quantitatively connected to the coupling V in Fermi's golden rule. NA coupling is responsible for the different time-scales of electron and hole relaxation rates, even in the presence of a symmetric DOS.

The applicability of Fermi's golden rule to the NA charge-phonon relaxation allows us to estimate the relaxation rates of electrons and holes in QDs by knowing the average NA coupling strength and the local DOS within the relevant energy range. We emphasize that the electron and hole relaxation dynamics produced by the current time-domain atomistic simulation is clearly more complex than the simple exponential decay implied by Fermi's golden rule. Relaxation includes exponential and Gaussian parts,[14,65] both of which cannot be described simultaneously by a simple perturbation theory such as Fermi's golden rule. The short time Gaussian relaxation switches to the exponential decay at longer times. Our time-domain atomistic simulations show that the latter component can be successfully described by Fermi's golden rule.

3.4. Phonon modes analysis

As we demonstrated above, with the nearly symmetric DOS, the NA couplings entirely determine the relative decay rates of electrons and holes. In order to rationalize the differences, we investigated the QD phonon modes that couple to the photoexcited charges. The left panels of figure 4 show the spectral densities (SD) of phonon-induced fluctuations of the energy levels of the CB and valence band (VB) states of $Si_{29}H_{24}$. The asymmetry in the NA couplings for the CB and VB can be rationalized by these higher-frequency components of the SD. Throughout all the shown frequencies, the SD of the CB states are significantly larger than the SD of the VB states. This result indicates that the stronger NA couplings for the electrons than holes are due to the stronger interaction between the CB states and the higher-frequency phonon modes of the Si-H bonds. Hence, it is the passivation of the QD surface with hydrogen ligands that produces the asymmetric NA couplings in the CB and VB. Since the NA coupling is proportional to the nuclear velocity, as in (4), the high-frequency phonon modes of the hydrogen ligands result in stronger NA couplings. Our results clearly show that surface ligands can significantly influence the charge relaxation processes.[72]

3.5. Charge delocalization over the surface bonds

The right panels of figure 4 support the conclusion that the difference in NA couplings for electrons and holes are attributed to the surface Si-H modes. The LUMO of the $Si_{29}H_{24}$ QD encompasses Si-H bonds more so than the HOMO, indicating that the electrons are more strongly coupled to the surface passivating bonds than the holes. The situation is different from materials such as CdSe, where the VB states are notably delocalized onto the surface, and holes are easily trapped there.[4,14] The ligand contribution to the electron and hole relaxation can emphasize the importance of the Auger energy exchange between the charge carriers, which accelerates the relaxation of the slower decaying carrier.[8] By changing the chemistry of the ligands, one can alter the strength of the NA coupling, and therefore, control the rates of energy losses in semiconductor QDs.

4. Phonon-induced dephasing dynamics of superpositions

Interactions with phonons make superpositions of electronic states dephase into uncorrelated states. In order to gain insights into the timescales of the dephasing processes, we characterize the phonon-induced dephasing for a variety of excitations at ambient and low temperatures in the indirect band-gap semiconductor QD, $Si_{29}H_{24}$. In particular, we consider dephasing of exciton pairs separated in energy by the band gap (Eg) and corresponding to the absorption and luminescence processes. We also investigate the lifetime of coherent superpositions of SEs and MEs encountered in MEG. Finally, we describe the dephasing that converts MEs into uncorrelated SEs, corresponding to MEF.

4.1. Types of excitation undergoing dephasing

A diagram of the representative dephasing processes is given in figure 5. The two states shown in each panel are in a coherent superposition initially and dephase by coupling to phonons. The two left panels illustrate superpositions of the ground state with the lowest energy SE, and the SE with the lowest energy DE. These superpositions are formed during light absorption and luminescence at the band gap energy. The dephasing of these superpositions determines the homogeneous linewidth of single molecule luminescence. The next two panels show superpositions of the high-energy SE and DE, and the high-energy SE and triexciton (TE). The high-energy SEs are near-resonant in energy with the band-gap DE and TE. Dephasing of these superpositions constitutes part of the MEG process. The right panel displays a biexciton fission diagram. Since the energy spacing between the orbitals is small, on the order of kT, we consider MEF into SEs that have different occupations of the orbitals near the band gap.

Table 1. Dephasing times (fs) at 80 K and 300 K for the processes drawn in figure 5

.

Process	80 K	300 K
Emit; DE/SE, SE/gr	6.98 ± 0.21	3.96 ± 0.10
MEG; $2E_g$/DE	7.33 ± 0.17	3.95 ± 0.13
MEG; $3E_g$/TE	2.96 ± 0.09	1.60 ± 0.05
MEF; $E_g/E_g^{e,h}$	205.33 ± 0.87	54.43 ± 1.06

4.2. Dephasing timescales

The dephasing functions, (10), calculated from the ACFs, (9), for the luminescence (SE/ground), MEG ($3E_g$/TE) and MEF ($E_g/E_g^{e,h}$) processes at 300 K and 80 K are plotted in figure 6. The dephasing times are listed in table 1. The dephasing times for luminescence and MEG are all sub-10fs, while the dephasing time of MEF is significantly longer, on the order of a hundred femtoseconds. The dephasing times are related to phonon-induced fluctuations of the energy gap between the two states through the linear response theory. The fluctuation of the large energy gaps corresponding to band gap absorption and luminescence produce fast dephasing. The gaps between SE and ME states involved in MEG are small. At the same time, these states are supported by orbitals that are far in energy. They depend quite differently on phonon coordinates; and as a result, the dephasing of SE and ME state pairs participating in MEG is also rapid. The orbitals supporting excitons undergoing MEF are very close in energy, leading to the much slower dephasing time. The MEF dephasing time caused by small fluctuations of the energy gaps should be sensitive to QD size, surface ligands, solvent, etc. The MEF dephasing time shows stronger temperature dependence than the other three dephasing times. This is because the MEF dephasing is facilitated by low-frequency acoustic phonons, while the luminescence and MEG dephasing occurs by coupling to high-frequency optical modes;[19] and low frequency phonon modes are more significantly affected by temperature decrease. As a result, the difference of the dephasing times for MEF compared to MEG and luminescence is more pronounced at the lower temperature. The inverse of the dephasing time for luminescence determines the homogeneous optical linewidth. Our data confirm the observation that the single-molecule luminescence lines are remarkably broad.[73] The linewidths deduced from the present theory are about 150 meV at room temperature and 80 meV at 80K, in agreement with the available experimental data.[74,75]

5. Multiple exciton generation and recombination dynamics in semiconductor quantum dots

Semiconductor QDs demonstrate the ability to generate multiple excitons by absorption of one high energy photon.[6–8,21,25–39] The initial photo-excitation creates superpositions

of SE and ME states, which rapidly dephase by coupling to phonons (see previous section). MEs generated immediately by photo-excitations correspond to the direct MEG mechanism.[76] SEs can create MEs by an Auger-type process that competes with electron-phonon relaxation (discussed in section 3). We investigated Auger-type MEG and MER dynamics in small Si QDs of different size and with different surface passivation, and compared the Si results with those for a CdSe QD.[5] Our earlier study focused on a Ge QD.[6]

5.1. Geometric and electronic structure of small QDs

The SE and DE DOS of the three small QDs, (A) Si_{10}, (B) Cd_6Se_6, and (C) $Si_{29}H_{24}$, are shown in figure 7. These three QDs allow us to investigate simultaneously the effects of material type, size, ligands, and excitation energy on the efficiency and mechanisms of the MEG and MER processes. Even these small clusters create a high density of SE and ME states. The DOS are smooth, similarly to the DOS of the larger CdSe QD shown in figure 3. The surface of the larger Si QD is passivated by hydrogens that eliminate unsaturated chemical bonds more efficiently than surface reconstruction alone. As a result, the HOMO-LUMO energy gap of the hydrogen-passivated Si QD is very close to the gaps of the smaller and bare Si and CdSe QDs; 2.0 eV, 2.0 eV, and 2.1 eV for Si_{10}, Cd_6Se_6, and $Si_{29}H_{24}$, respectively even though the gap is generally inversely proportional to the QD diameter.[26,48–50] The DOS is clearly larger in $Si_{29}H_{24}$ than in the smaller QDs, as seen in the y-axis scales of the different panels. The DE DOS starts at higher energy than the SE DOS, but the former rapidly becomes dominant due to the increasing combinatorial number of DEs with energy. The ratio of the DE DOS to the SE DOS is largest for $Si_{29}H_{24}$ at high energies. The analysis of the SE and DE DOS suggests that excited state population will shift to DEs at high energies and to SEs at low energies.

The geometric and electronic structures of the QDs are illustrated in the inserts of figure 7. The left-most panels present geometry snapshots from the dynamics simulation at ambient temperature. All QDs preserve the original bulk topology at room temperature, bonds do not break, and defect states do not appear within the gap. The middle and right panels of the inserts display the HOMO and LUMO charge densities. The orbitals of the smaller cluster appear notably more localized, compared to the $Si_{29}H_{24}$ QD where the HOMO and LUMO are delocalized over the core region due to the more homogeneous bonding pattern. The hydrogen ligands passivating the $Si_{29}H_{29}$ surface affect the orbitals; the LUMO is delocalized over the hydrogen ligands more substantially than the HOMO.

5.2. Multiple exciton generation

Through the decay of the total population of all SEs, MEs appear starting from an initially excited SE as shown in figure 8. Our simulation includes SEs, DEs, and the ground state, but the ground state population remains negligible throughout several

picoseconds of the NAMD simulation, in agreement with the experiments.[73,77–79] The MEG dynamics studied here strongly depend on the initial excitation energy as reported in the experiments.[6,31–39,44] The energy dependence of the MEG rates arises mainly from the rapid increase of the DE DOS with energy, figure 7. The MEG dynamics is faster in Si_{10} than Cd_6Se_6, as indicated by the lines (A) and (B) in the upper-left panel of figure 8. This is because the ratio of the DE DOS over the SE DOS is larger in the former than in the latter QD.

Most other theories focus on MEG rates by assuming an exponential MEG process.[25,31–34,38,39,44,58] The transitions from the Gaussian to the exponential regime occur when the number of quantum states accessible to system's dynamics becomes large. The MEG dynamics in the smaller QDs are well fitted by the Gaussian functions, indicating that the DE DOS that couple to the SE states is relatively small, and that a rate description, such as Fermi's golden rule requiring a high density of final states, is not applicable there. On the other hand, the MEG data for the large QD can be fitted by a combination of Gaussian and exponential functions because sufficiently many DEs participate in the MEG dynamics at a later time.

Our NAMD study explicitly includes phonon dynamics, and therefore allows for phonon-assisted Auger processes. Indeed, we demonstrated the phonon-assisted MEG starting at energies lower than $2E_g$, as seen in the left-lower panel of figure 8. The high frequency Si-H phonon modes in the $Si_{29}H_{24}$ QD enabled this phonon-assisted MEG: the electronic degrees of freedom can borrow energy from high energy phonons and allow MEG even below the purely electronic threshold.

5.3. Phonon modes involved in MEG and MER

In order to characterize the phonon modes that couple SE and ME states, we computed the Fourier transforms of the corresponding, time-dependent energy gaps. The electronic energies fluctuate due to coupling to phonons, and the energy gap fluctuation is directly related to the electron-phonon coupling.[80] The spectra for the three QDs are presented in the right panels of figure 8. The Si_{10} phonons are higher in frequency than the Cd_6Se_6 phonons, accelerating the faster MEG dynamics in the Si_{10} QD. The light hydrogen atoms passivating the surface of the $Si_{29}H_{24}$ QD introduce additional high frequency modes up to 2000 cm^{-1}, increasing the efficiency of phonon-assisted MEG. The ligand contribution to the QD electronic states and electron-phonon coupling should decrease with increasing QD size due to the reduced surface-to-volume ratio.

5.4. Interplay between MEG and MER dynamics

Our simulation involves simultaneously a variety of processes, enabling us to study the interplay between MEG and MER, and to provide additional physical details of the combined MEG/MER dynamics.

The left panel of figure 9 shows a two-dimensional (2D) energy representation of the dynamics of two SEs that form a DE, reflecting the diffusion of the two SEs in

the energy manifold of the $Si_{29}H_{24}$ QD. At early times, 0.01 ps, the photoexcited high energy SE undergoes MEG, forming few DEs. The DEs appear asymmetrically, rather than around the center of the 2D map, supporting the impact ionization mechanism and the experimental expectations.[7,8,26,31–34] The second SE in $Si_{29}H_{24}$ is created at the energy that is slightly higher than E_g=2.1 eV. This can be attributed to the entropic effect: while it is more favorable energetically to create the second exciton close to E_g, the rapid increase of the DE DOS with energy in the larger QD makes the second SE appear at the slightly higher energy. The initial asymmetric SEs diffuse along the constant energy line towards the center of the 2D map, where the two SEs forming a DE have similar energies. This process is also driven entropically, since there exist many more possibilities to distribute energy roughly equally between the two SEs, rather than to maintain a high and a low energy SE.

The right panel of figure 9 shows the SE population dynamics accompanying the DE generation displayed in the left panel. The data are plotted as a 2D function of time and energy. The initial SE evolves into other SEs, and at around 1 ps, the total SE population becomes small as a result of the MEG, in harmony with the accelerating MEG in figure 8. Comparison of the left and right panels in figure 9 indicates that MEG (right panel) is faster than the subsequent diffusion of the generated pair of SEs in the manifold of DE states (left panel). The SE population starts to reappear at a lower energy after 1.5 ps-2 ps. This population recursion directly reflects MER, demonstrating that our approach simultaneously takes into account both MEG and MER. The MER time of 1.5 ps-2 ps agrees with the experimental results for small QDs.[26,48–50] In comparison, MER starting from a single DE state takes several hundred picoseconds.[5,6,31,33,34,44] A superposition of many DEs produced by the preceding MEG process enables multiple coupling pathways to a broader range of SEs, producing much more reasonable timescale estimates. In other words, the MEG is more efficient than the diffusion from the initially excited single DE. This effect is particularly pronounced for MER compared to MEG, since the density of final SE states in MER is much lower than the density of final DE states in MEG, and it is important to couple to as many final states as possible in order to achieve efficient MER.

6. Concluding remarks

In summary, we developed and performed a time-domain, atomistic, *ab initio* studies of photoexcited carrier relaxation, MEG, MEF, and MER dynamics in small semiconductor QDs of different size and material, with and without ligands. Since these photoexcited dynamic processes dominate excitation and charge dynamics in most nanoscale systems, the developed approach can find many applications in the future. Our atomistic method is very well suited to investigate defects, ligands, charges, dopants and dangling bonds, which could play extremely important roles in excitation dynamics of QDs.

Ligands passivating the QD surface accelerate electron-phonon relaxation due to enhancement of the NA electron-phonon coupling by the high-frequency ligand

modes. In particular, hydrogen ligands passivating the Si QD surface couple strongly to electrons, but not holes. As a result, electrons relax in energy several times faster than holes, in spite of the nearly symmetric electron-hole band structure. Ligands eliminate surface states, minimizing trapping of charge carriers and enhancing the contribution of Auger-type energy exchange between electrons and holes to the overall energy relaxation. By selecting a ligand, one should be able to control and manipulate, to a large extent, charge carrier relaxation in semiconductor QDs.

Our explicit time-domain study shows that the initial stage of energy decays is Gaussian, and that exponential relaxation ensues once the quantum dynamics spreads over a sufficiently large number of states. The Gaussian component is particularly important in small QDs with a relatively low density of states. The rate of the exponential decay can be well described by Fermi's golden rule formulated in terms of the NA electron-phonon coupling and DOS averaged over the relevant energy range. Our study provides a justification for perturbative description of relaxation processes in semiconductor QDs.

We investigated the phonon-induced pure-dephasing processes that contribute to the photoinduced dynamics of electronic excitations in semiconductor QDs. In particular, we considered the dephasing that determines the homogeneous width of optical absorption and emission lines, the lifetime of coherent superpositions of single and MEs formed during MEG and MER, and fission of MEs into independent SEs. The dephasing of MEF is much longer than the other dephasing processes due to the small energy differences in the excitons involved in MEF. The dephasing leading to MEF is facilitated by low-frequency phonon modes, while both low- and high-frequency modes contribute to the other dephasing processes.

By explicitly coupling the ground, SE and DE electronic states to phonon motions, we developed an *ab initio* time-domain modeling of Auger and phonon-assisted Auger processes in semiconductor nanocrystals. The time-domain representation describes the various MEG regimes, bypassing the limitations of rate models that implicitly assume exponential decay. The MEG timescale showed strong energy dependence, in agreement with available experimental and theoretical data. The energy dependence of the interplay of MEG and MER dynamics is determined by the relative densities of SE and ME states, with the MEG threshold corresponding to the crossing between these DOS. The MEG and MER timescales depend both on the DOS and the strength of coupling between SEs and MEs. The coupling in particular, shows complex dependence on energy, QD size and material. Efficient MER, in agreement with the experimental data, was observed by virtue of the superposition of many DEs, produced during the preceding MEG process, enabling ME couplings to a broad range of SEs. Ligand modes are particularly important for phonon-assisted Auger processes, since they provide the highest frequency phonons capable of exchanging significant amounts of energy with the electronic subsystem.

Our studies provided the first direct evidence that the phonon modes of the passivated QD surfaces play a vital function in the photoexcited carrier dynamics

in semiconductor QDs. Therefore, carefully controlled synthetic inorganic chemistry involving reactions between inorganic semiconductors and molecular ligands is a very valuable tool needed for advancing experimental aspects of QD research aimed at efficient harvesting and conversion of solar energy. The insights reported here enhance our understanding of the properties and behavior of nanoscale materials in general, and create valuable guidelines for development of photovoltaic, electronic, lasing, spintronic, bio-imaging and other devices.

Acknowledgments

KHD is partially supported by KAKENHI No. 24750016. OVP acknowledges financial support of DOE, grant no. DE-FG02-05ER15755, dedicated to the QD studies, and NSF, grant no. CHE-1050405, supporting the method developments.

References

[1] Bester G 2009 *J. Phys. Cond. Matt.* **21** 023202.
[2] Mackowski S 2010 *J. Phys. Cond. Matt.* **22** 193102.
[3] Nozik A J 2001 *Ann. Rev. Phys. Chem.* **52** 193–231.
[4] Pandey A and Guyot-Sionnest P 2008 *Science* **322** 929–932.
[5] Hyeon-Deuk K and Prezhdo O V 2012 *ACS Nano* **6** 1239–1250.
[6] Hyeon-Deuk K and Prezhdo O V 2011 *Nano Lett.* **11** 1845–1850.
[7] Schaller R D and Klimov V I 2004 *Phys. Rev. Lett.* **92** 186601.
[8] Ellingson R J, Beard M C, Johnson J C, Yu P R, Micic O I, Nozik A J, Shabaev A and Efros A L 2005 *Nano Lett.* **5** 865–871.
[9] McGuire J A, Joo J, Pietryga J M, Schaller R D and Klimov V I 2008 *Acc. Chem. Res.* **41** 1810–1819.
[10] Prezhdo O V 2008 *Chem. Phys. Lett.* **460** 1–9.
[11] Shockley W and Queisser H J 1961 *J. Appl. Phys.* **32** 510–519.
[12] Knowles K E, McArthur E A and Weiss E A 2011 *ACS Nano* **5** 2026–2035.
[13] Sykora M, Koposov A Y, McGuire J A, Schulze R K, Tretiak O, Pietryga J M and Klimov V I 2010 *ACS Nano* **4** 2021–2034.
[14] Kilina S V, Kilin D S and Prezhdo O V 2009 *ACS Nano* **3** 93–99.
[15] Lupo M G, Della Sala F, Carbone L, Zavelani-Rossi M, Fiore A, Luer L, Polli D, Cingolani R, Manna L and Lanzani G 2008 *Nano Lett.* **8** 4582–4587.
[16] Schaller R D, Pietryga J M, Goupalov S V, Petruska M A, Ivanov S A and Klimov V I 2005 *Phys. Rev. Lett.* **95** 196401.
[17] Cooney R R, Sewall S L, Anderson K E H, Dias E A and Kambhampati P 2007 *Phys. Rev. Lett.* **98** 177403.
[18] Hyeon-Deuk K and Prezhdo O V 2009 *Dalton Trans.* **45** 10069–10077.
[19] Madrid A B, Hyeon-Deuk K and Prezhdo O V 2009 *ACS Nano* **3** 2487–2494.
[20] Lanzani G, Cerullo G, Zavelani-Rossi M, De Silvestri S, Comoretto D, Musso G and Dellepiane G 2001 *Phys. Rev. Lett.* **87** 187402.
[21] Murphy J E, Beard M C, Norman A G, Ahrenkiel S P, Johnson J C, Yu P R, Micic O I, Ellingson R J and Nozik A J 2006 *J. Am. Chem. Soc.* **128** 3241–3247.
[22] Shabaev A, Efros A L and Nozik A J 2006 *Nano Lett.* **6** 2856–2863.
[23] Nozik A J 2002 *Physica E* **14** 115–120.
[24] Nozik A J 2008 *Chem. Phys. Lett.* **457** 3–11.

[25] Schaller R D, Agranovich V M and Klimov V I 2005 *Nature Phys.* **1** 189–194.
[26] Schaller R D, Pietryga J M and Klimov V I 2007 *Nano Lett.* **7** 3469–3476.
[27] Beard M C, Knutsen K P, Yu P R, Luther J M, Song Q, Metzger W K, Ellingson R J and Nozik A J 2007 *Nano Lett.* **7** 2506–2512.
[28] Beard M C, Midgett A G, Law M, Semonin O E, Ellingson R J and Nozik A J 2009 *Nano Lett.* **9** 836–845.
[29] Ji M, Park S, Connor S T, Mokari T, Cui Y and Gaffney K J 2009 *Nano Lett.* **9** 1217–1222.
[30] Lin Z, Franceschetti A and Lusk M T 2011 *ACS Nano* **5** 2503–2511.
[31] Franceschetti A, An J M and Zunger A 2006 *Nano Lett.* **6** 2191–2195.
[32] Luo J W, Franceschetti A and Zunger A 2008 *Nano Lett.* **8** 3174–3181.
[33] Rabani E and Baer R 2008 *Nano Lett.* **8** 4488–4492.
[34] Rabani E and Baer R 2010 *Chem. Phys. Lett.* **496** 227–235.
[35] Isborn C M, Kilina S V, Li X and Prezhdo O V 2008 *J. Phys. Chem. C* **112** 18291–18294.
[36] Fischer S A, Isborn C M and Prezhdo O V 2011 *Chem. Sci.* **2** 400–406.
[37] Califano M 2009 *ACS Nano* **3** 2706–2714.
[38] Piryatinski A and Velizhanin K A 2010 *J. Chem. Phys.* **133** 084508.
[39] Califano M 2011 *ACS Nano* **5** 3614–3621.
[40] Semonin O E, Luther J M, Choi S, Chen H-Y, Gao J, Nozik A J and Beard M C 2011 *Science* **334** 1530–1533.
[41] Ueda A, Matsuda K, Tayagaki T and Kanemitsua Y 2008 *Appl. Phys. Lett.* **92** 233105.
[42] Wang S, Khafizov M, Tu X, Zheng M and Krauss T D 2010 *Nano Lett.* **10** 2381–2386.
[43] Gabor N M, Zhong Z, Bosnick K, Park J and McEuen P L 2009 *Science* **325** 1367–1371.
[44] Baer R and Rabani E 2010 *Nano Lett.* **10** 3277–3282.
[45] Johnson J C, Nozik A J and Michl J 2010 *J. Am. Chem. Soc.* **132** 16302–16303.
[46] Beard M C, Midgett A G, Hanna M C, Luther J M, Hughes B K and Nozik A J 2010 *Nano Lett.* **10** 3019–3027.
[47] Huang L B and Krauss T D 2006 *Phys. Rev. Lett.* **96** 057407.
[48] Robel I, Gresback R, Kortshagen U, Schaller R D and Klimov V I 2009 *Phys. Rev. Lett.* **102** 177404.
[49] Kobayashi Y, Pan L and Tamai N 2009 *J. Phys. Chem. C* **113** 11783–11789.
[50] Kobayashi Y, Nishimura T, Yamaguchi H and Tamai N 2011 *J. Phys. Chem. Lett.* **2** 1051–1055.
[51] Jha P P and Guyot-Sionnest P 2009 *ACS Nano* **3** 1011–1015.
[52] Ivanov S A and Achermann M 2010 *ACS Nano* **4** 5994–6000.
[53] Sambur J B, Novet T and Parkinson B A 2010 *Science* **330** 63–66.
[54] Nair G and Bawendi M G 2007 *Phys. Rev. B* **76** 08134.
[55] Nair G, Geyer S M, Chang L-Y and Bawendi M G 2008 *Phys. Rev. B* **78** 125325.
[56] Trinh M T, Houtepen A J, Schins J M, Hanrath T, Piris J, Knulst W, Goossens A P L M and Siebbeles L D A 2008 *Nano Lett.* **8** 1713–1718.
[57] Ben-Lulu M, Mocatta D, Bonn M, Banin U and Ruhman S 2008 *Nano Lett.* **8** 1207–1211.
[58] Pijpers J J H, Ulbricht R, Tielrooij K J, Osherov A, Golan Y, Delerue C, Allan G and Bonn M 2009 *Nature Phys.* **5** 811–814.
[59] McGuire J A, Sykora M, Joo J, Pietryga J M and Klimov V I 2010 *Nano Lett.* **10** 2049–2057.
[60] Tyagi P and Kambhampati P 2011 *J. Chem. Phys.* **134** 094706.
[61] Craig C F, Duncan W R and Prezhdo O V 2005 *Phys. Rev. Lett.* **95** 163001.
[62] Prezhdo O V 2009 *Acc. Chem. Res.* **42** 2005–2016.
[63] Kresse G and Furthmuller J 1996 *Comp. Mat. Sci.* **6** 15–50.
[64] Craig C F, Duncan W R and Prezhdo O V 2005 *Phys. Rev. Lett.* **95** 163001.
[65] Kilina S V, Craig C F, Kilin D S and Prezhdo O V 2007 *J. Phys. Chem. C* **111** 4871–4878.
[66] Parandekar P V and Tully J C 2005 *J. Chem. Phys.* **122** 094102.
[67] Prezhdo O V, Duncan W R and Prezhdo V V 2009 *Prog. Surf. Sci.* **84** 30.
[68] Mukamel S 1995 *Principles of Nonlinear Optical Spectroscopy* (New York: Oxford University Press)

[69] Klimov V I, Mikhailovsky A A, McBranch D W, Leatherdale C A and Bawendi M G 2000 *Phys. Rev. B* **61** R13349–R13352.
[70] Guyot-Sionnest P, Wehrenberg B L and Yu D 2005 *J. Chem. Phys.* **123** 074709.
[71] See http://cms.mpi.univie.ac.at/vasp-workshop/slides/handsonII.pdf.
[72] Prezhdo O V and Rossky P J 1996 *J. Phys. Chem.* **100** 17094.
[73] Peterson J J and Krauss T D 2006 *Nano Lett.* **6** 510–514.
[74] Valenta J, Juhasz R and Linnros J 2002 *Appl. Phys. Lett.* **80** 1070–1072.
[75] Sychugov I, Juhasz R, Valenta J and Linnros J 2005 *Phys. Rev. Lett.* **94** 087405.
[76] Fischer S A, Isborn C M and Prezhdo O V 2011 *Chemical Science* **2** 400.
[77] Nirmal M, Dabbousi B O, Bawendi M G, Macklin J J, Trautman J K, Harris T D and Brus L E 1996 *Nature* **383** 802–804.
[78] Sykora M, Mangolini L, Schaller R D, Kortshagen U, Jurbergs D and Klimov V I 2008 *Phys. Rev. Lett.* **100** 067401.
[79] Moreels I, Lambert K, Smeets D, DeMuynck D, Nollet T, Martins J C, Vanhaecke F, Vantomme A, Delerue C, Allan G and Hens Z 2009 *ACS Nano* **3** 3023–3030.
[80] Miller W H and George T F 1972 *J. Chem. Phys.* **56** 5637–5652.

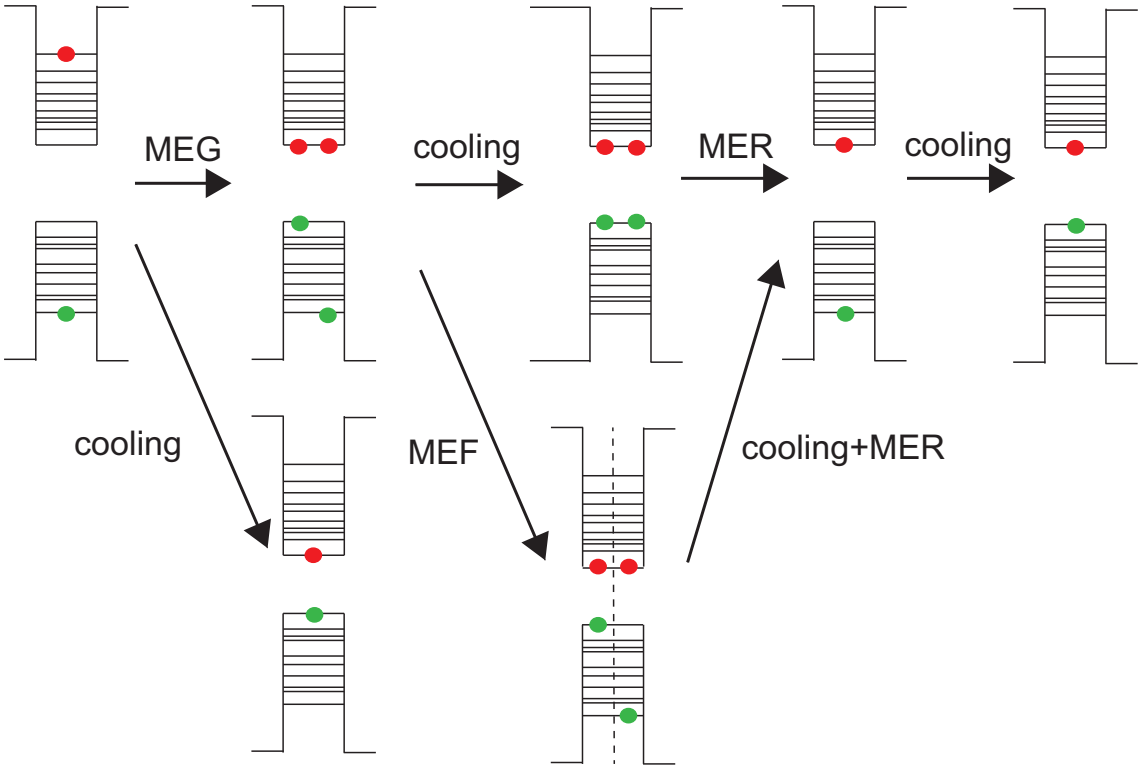

Figure 1. Photoexcited processes in a semiconductor QD discussed in this review. An initially excited electron-hole pair of high energy can generate another electron and hole pair, MEG. MEG competes with charge-phonon nonradiative relaxation, converting excitation energy to heat. Multiple electron-hole pairs dephase into independent single electron-hole pairs by couplings to phonons, MEF. Lower energy multiple exciton states undergo MER. Ultimately, all processes lead to a long-lived electron-hole pair at the band gap energy.

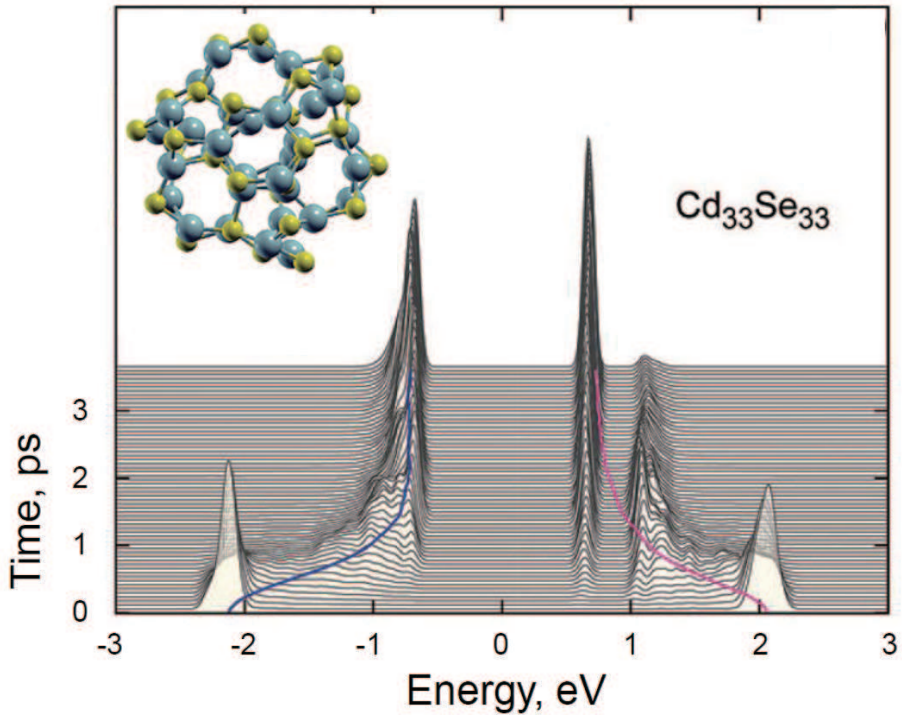

Figure 2. Population relaxation dynamics of the electron (magenta line) and hole (blue line) in the $Cd_{33}Se_{33}$ QD with no surface passivation.[14] The phonon bottleneck appears around the band edge of CB.

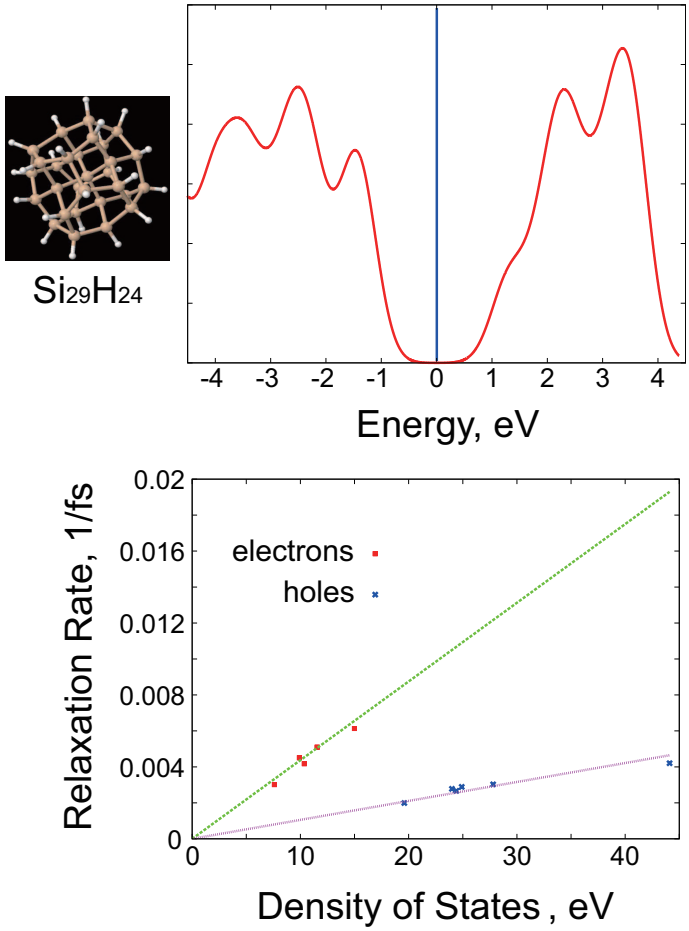

Figure 3. (Upper panel) Density of electron and hole states in the $Si_{29}H_{24}$ QD. Quantum confinement makes the CB and VB DOS more symmetric than the corresponding bulk DOS, in contrast with other semiconductor QDs such as CdSe. (Lower panel) Linear relationships found in the ultrafast electron and hole relaxations in $Si_{29}H_{24}$. In spite of the symmetric DOS (upper panel), the relaxation is asymmetric. Electrons relax more rapidly than holes; and the rate of electron relaxation grows faster with DOS, which depends on the excitation energy.

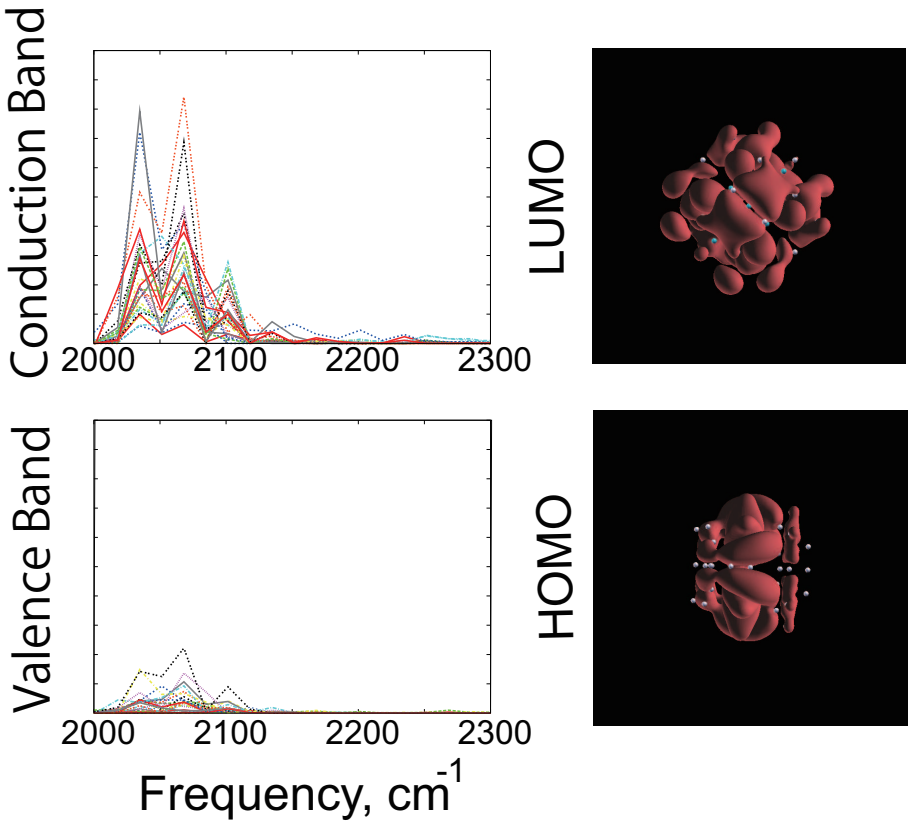

Figure 4. Phonon SD for the CB (upper-left panel) and VB (lower-left panel) states of the $Si_{29}H_{24}$ QD. The y-axis scale is arbitrary but the same in both panels. The SD of CB are clearly larger than the SD of VB, indicating a stronger phonon coupling to electrons than holes. HOMO and LUMO charge densities of the $Si_{29}H_{24}$ QD (right panels). LUMO is delocalized onto and has higher density around the passivating Si-H bonds than HOMO, rationalizing the stronger coupling of electrons to the surface phonon modes.

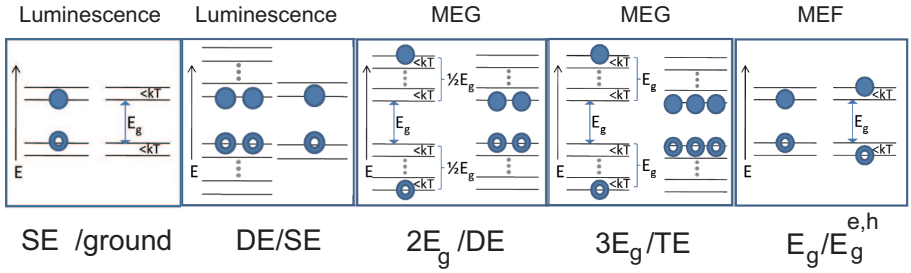

Figure 5. Diagram of electronic state pairs undergoing phonon-induced dephasing. (Left panel) Superposition of the lowest excited and ground states. (Mid-left panel) superposition of the lowest DE and SE states. (Middle panel) superposition of double band gap exciton ($2E_{\mathrm{g}}$) and DE involved in MEG. (Mid-right panel) superposition of triple band gap exciton ($3E_{\mathrm{g}}$) and TE involved in MEG. (Right panel) superposition of SEs within kT of the band gap involved in MEF.

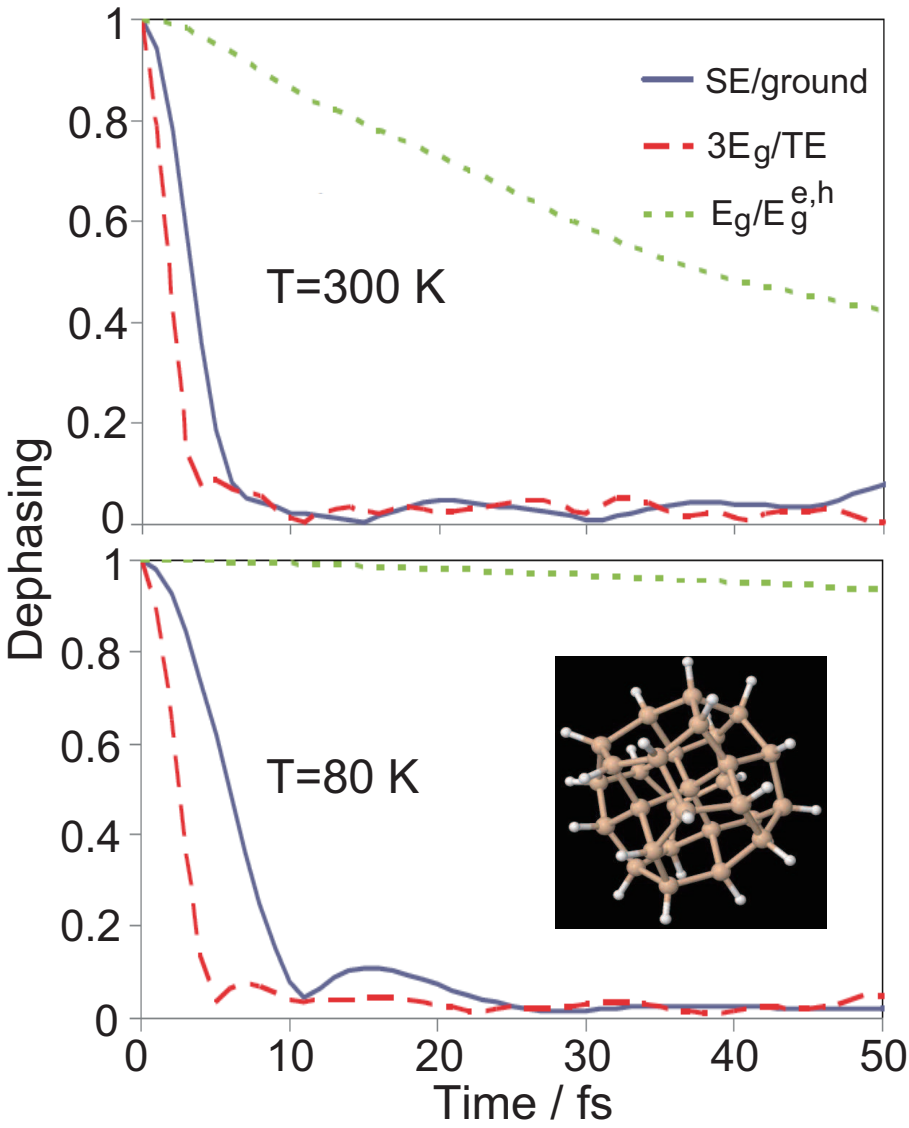

Figure 6. Dephasing functions for the three processes corresponding to figure 5. Dephasing times obtained by Gaussian fittings are presented in table 1 and are discussed in the main text.

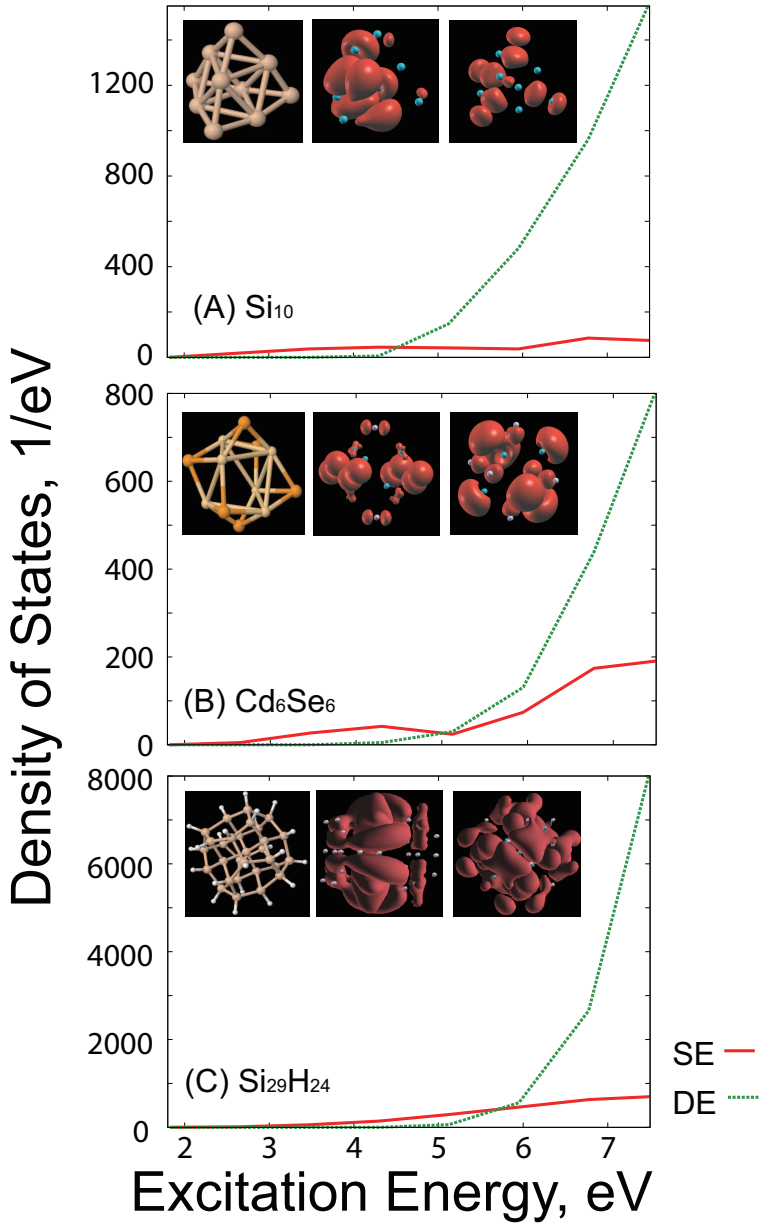

Figure 7. SE and DE DOS of (A) Si_{10}, (B) Cd_6Se_6, and (C) $Si_{29}H_{24}$. The DE DOS starts at higher energies than the SE DOS, but the former rapidly overtakes the latter as the energy increases. The DOS is much higher in $Si_{29}H_{24}$ than in the smaller QDs, and the DE/SE DOS ratio increases most rapidly. Typical structures from a dynamics trajectory at the ambient temperature, and charge densities of the HOMO and LUMO states are shown from left to right in each panel.

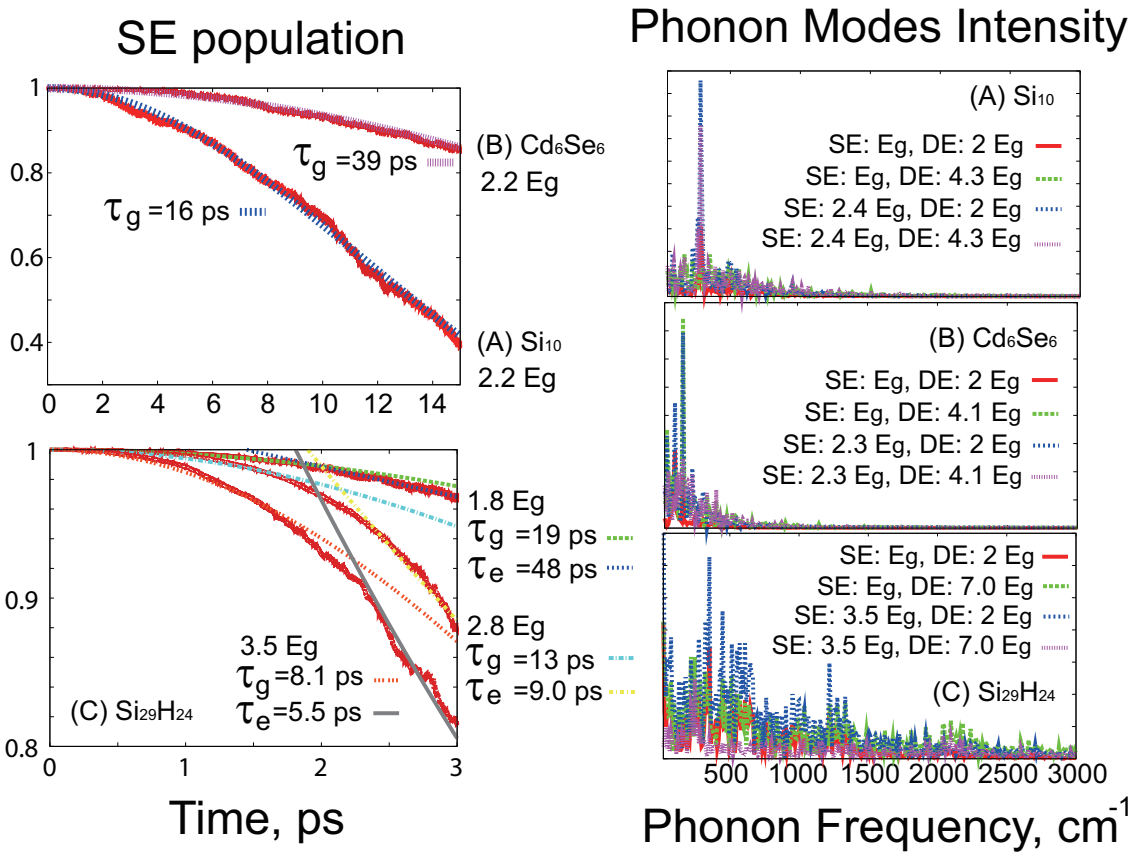

Figure 8. (Left panels) Total population of all SEs starting from an initially excited SE of the displayed energy. The population decrease due to MEG. MEG follows Gaussian decay in the smaller clusters, while MEG in $Si_{29}H_{24}$ exhibits a transition from the Gaussian to the exponential decay. Slow phonon-assisted MEG is observed at energies below $2E_g$ in $Si_{29}H_{24}$. The Gaussian and exponential timescales, τ_g and τ_e, are displayed. MEG is faster in Si_{10} than in Cd_6Se_6, reflecting the larger DE/SE ratio in Si_{10} around 2.2 E_g (see figure 7). (Right panels) Phonon modes that couple the SE and DE pairs displayed in the figure. The phonon peaks appear at higher energies in lighter Si_{10} than in heavier Cd_6Se_6, supporting the faster MEG in Si_{10}. $Si_{29}H_{24}$ exhibits a broader phonon spectrum, and possesses high-frequency Si-H phonon modes, leading to the efficient phonon-assisted MEG.

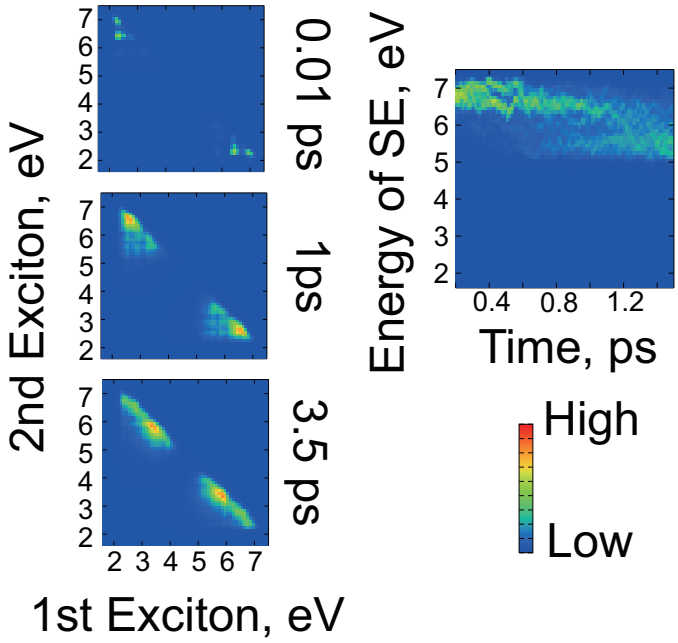

Figure 9. (Left panels) Evolution of the two excitons forming DE states that appear in $Si_{29}H_{24}$ as a resuls of MEG. The two SEs are asymmetric in energy, with the second SE appearing around the band gap energy, in agreement with the impact ionization mechanism. The SE pair evolves into other SE pairs along the constant energy line. (Right panel) SE population dynamics accompanying the DE dynamics shown in the left panels. The initially excited SE evolves into other SE and DE states. The decrease in the SE population seen at intermediate times corresponds to MEG shown in figure 8. The recursion of the SE population at a later time corresponds to MER, demonstrating that our method accounts for MEG and MER simultaneously. The obtained MER timescale of 1 ps to 3 ps agrees with the experimental observations for small QDs.[26,48–50]